Physica A 509 (2018) 1162–1173

Contents lists available at ScienceDirect

Physica A

journal homepage: www.elsevier.com/locate/physa

Wavefront-obstacle interactions and the initiation of reentry in excitable media

Zahra Rostami [a,*], Karthikeyan Rajagopal [b], Abdul Jalil M. Khalaf [c], Sajad Jafari [a], Matjaž Perc [d,e], Mitja Slavinec [d]

[a] Biomedical Engineering Department, Amirkabir University of Technology, Tehran 15875-4413, Iran
[b] Center for Nonlinear Dynamics, College of Engineering, Defence University, Ethiopia
[c] Ministry of Higher Education and Scientific Research, Baghdad, Iraq
[d] Faculty of Natural Sciences and Mathematics, University of Maribor, Koroška cesta 160, SI-2000 Maribor, Slovenia
[e] School of Electronic and Information Engineering, Beihang University, Beijing 100191, China

HIGHLIGHTS

- The proper rhythm of cardiomyocyte's constriction can be broken by the obstacles.
- Electrical patterns resulting from the wavefront-obstacle interaction are studied.
- The resulting interaction can give rise to reentry and spiral waves.
- The obstacle towards the direction of wave propagation causes spatial deformation.
- The continuity of successive plane waves, in turn, determines the spatial patterns.

ARTICLE INFO

Article history:
Received 29 May 2018
Available online xxxx

Keywords:
Obstacle
Reentry
Cardiac arrhythmia
Spatiotemporal pattern

ABSTRACT

The combination of the heart's electrical and mechanical activities gives rise to complex dynamics. The reentry, which is one of the most prominent types of heart arrhythmias, is the result of an abnormal electrical activity in the cardiac tissue. These abnormalities are often associated with local non-excitable or partially excitable areas in the cardiac tissue called obstacles. In fact, the proper rhythm for the constriction of cardiomyocytes can be broken by these abnormal obstacles. In this study, we investigate the electrical patterns in a model of excitable media resulting from the interaction between the obstacle and the wavefronts. We consider a slice of cardiac tissue with a rectangular obstacle in vertical and horizontal orientation. Our research reveals that the interaction of the wavefront-obstacle can give rise to reentry and spiral waves. It is also found that a wider section of the obstacle towards the direction of wave propagation causes more deformation in the spatial patterns. In addition, since it can postpone reentry, the continuity of the successive plane waves also determines the resulting spatial patterns.

1. Introduction

The heart is a vital organ responsible for pumping blood to the body. The heart ventricles support both normal rhythm and ventricular fibrillation, and thus have bistability [1]. In the cardiac tissue, the cardiomyocytes conduct the electrical

* Corresponding author.
E-mail address: z.rostami.zrmi@gmail.com (Z. Rostami).

https://doi.org/10.1016/j.physa.2018.06.062
0378-4371/

pulses generated from the sinoatrial (SA) node in a proper sequence. The electrical activity of the heart determines its mechanical activity and leads to constriction of the heart's muscle fibers. Therefore, the normal constriction of the heart muscle relies on the normal rhythm of successive electrical excitations. This mechanism, in turn, makes the heart's both electrical and mechanical function complicated. On the other hand, the cardiac tissue is not homogeneous. It normally contains some structures with the excitability properties that are different from other parts. These partially excitable or non-excitable regions called obstacles are not detrimental in general, which the wavefront simply goes around and then continues to pass [2]. However, the proper rhythm of the constriction of the cardiomyocytes can also be broken by the obstacle or heterogeneity under some abnormal circumstances. These abnormalities arise from different mechanisms such as inadequate blood supply to a local area of the tissue and myocardial infarction [3], tumor pressure on the blood vessels or nerves, prolonged refractory period in a local region [3], a reduced excitability or even inexcitability of the medium [2], the sodium channels blocked by some drug effects [3], etc. Furthermore, in the nervous system, the continuous pulses can originate from anatomical heterogeneity, so that the normal signal propagation is stopped [4]. The studies show that cardiac arrhythmias leading to ventricular fibrillation are often associated with abnormal obstacles or heterogeneities. In fact, the obstacles play an essential role in initiation of reentry [5], which is the most prominent type of the heart arrhythmias [6]. Therefore, the wavefront-obstacle interaction is important to be studied. In addition, in [7], there is an experimental and theoretical study on various types of reentrant rhythms in a monolayer cardiac tissue.

Patten formation in an excitable media is frequently investigated by mathematical modeling. In this regard, the effects of different factors such as noise [8], the number of coupling channels [9], the connection type [10], and the time delay [11] on the spatiotemporal order of the excitable media are examined. Cardiac electrical activity is often studied by recognition of the propagating wave patterns in the cardiac tissue. The significance of these studies is well noticed while these patterns arise from both local dynamics of the cells and also the impulse connection between them through the gap junctions. The aim is to probe the normal and abnormal function of the heart from theoretical or experimental perspective. For example, the cardiac electrical waves normally are originated from the SA node; however, some other pulse origins aside from the SA node can emerge by the abnormalities. One type of these abnormal sources is the rotating spiral seed that generates expanding circular waves [12]. Spiral waves are important to be studied while they substantially underlie the reentrant excitation in the cardiac tissue [5]. When a spiral seed emerges in the cardiac tissue, it rotates with a higher frequency compared to the natural frequency of the heart's pacemaker. This makes the heartbeat rapid and irregular. The high-frequency arrhythmias are often a reason of fibrillation and cardiac death. Furthermore, the situation gets worse when the spiral seed is unstable and breaks up to multiple spiral seeds, and each of them has its own rotation frequency. This puts the heart in a turbulent manner and a desynchronized state called fibrillation [12,13]. Subsequently, the synchronized mechanical constriction of the heart muscle stops, and thus the sufficient pumping blood is lost. The sudden heart death is often associated with heterogeneity and obstacles [3], nevertheless, the connection between the cardiac arrhythmias, reduced excitability, and the obstacles is still controversial.

Some studies confirm that, the obstacles in cardiac tissue stabilize the spiral wave dynamics [14–17], while other studies argue that the obstacles can also act as destabilizers [18]. Olmos-Liceaga et al. focused on finding the minimum size obstacle that permits generation of the spiral and scroll waves in an excitable media [19]. Zhang et al. studied the effect of heterogeneity and its neighbor area on spiral waves using a cardiac model [20]. In their study a circular heterogeneity is considered by blocking the potassium ion channel, and then the nearby rotating spiral seed is located. Lim et al. confirmed that the spiral waves can become anchored in cardiac tissue due to the anatomic obstacles [21]. Athill et al. investigated the meandering functional reentry, a mechanism of cardiac arrhythmia, in the atrium [22]. Cysyk and Tung studied the effect of electric field on the obstacle, because the spiral waves are anchored by the obstacle, and this can lead to ventricular fibrillation and sudden cardiac death [23].

In this paper, we investigate the reentry and the formation of spiral waves in the cardiac tissue in the presence of a partially excitable obstacle. We use an enhanced version of the FHN model in which the magnetic flux is considered. This is because, in the real neuron, the continuous exchange of the ions across the membrane causes a time-varying magnetic field. The time-varying magnetic field also affects the membrane's electrical activity. In our study, the induction current affecting the neuron's membrane potential and the inhibitory property of the neuron's dynamics are the two factors that we use to adjust the tissue's excitability. After that, we consider a rectangular obstacle in the tissue in the presence of both continuous and intermittent traveling plane waves to investigate the wavefront-obstacle interaction. The results show that the reentrant excitation takes place near the obstacle's borders and potentially leads to multi-spirals in that area. We place both vertical and horizontal obstacles and generate successive wavefronts from the tissue's left boundary. The aim is to examine two different orientations of the obstacle toward the propagation direction. We found that a wider section of the obstacle toward the wave propagation direction brings more deformation for the spatial patterns. Furthermore, aside from the obstacle's orientation, the strength and the continuity of the successive plane waves also determines the resulting spatial patterns. In fact, it can postpone the reentry, and thus there can be less deformation in the normal spatial pattern. Our study also confirms that the high excitability of the tissue causes the plane waves transfer easier in the tissue.

The rest of the paper is organized as follows:

In the next section, we represent the mathematical model that we use for our simulations. In Section 3 the detailed explanation of our numerical study is given. Furthermore, the simulation results are shown in this section. Finally, the conclusion of our work can be found in Section 4.

Table 1
The parameters settings for Figs. 1–3.

Figures	Parameters
Fig. 1a–e	$\varepsilon = 0.02$ $k_0 = -1$
Fig. 1f–j	$\varepsilon = 0.002$ $k_0 = -1$
Fig. 2a–e	$\varepsilon = 0.02$ $k_0 = -0.5$
Fig. 2f–j	$\varepsilon = 0.002$ $k_0 = -0.5$
Fig. 3a–e	$\varepsilon = 0.02$ $k_0 = 0.5$
Fig. 3f–j	$\varepsilon = 0.002$ $k_0 = 0.5$

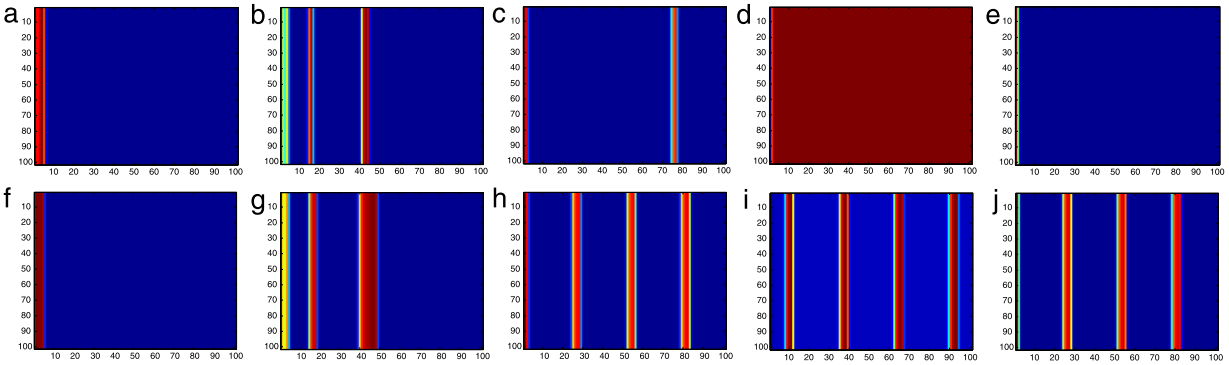

Fig. 1. Intermittent and continuous plane waves, traveling across the excitable tissue; for (a–e) $\varepsilon = 0.02$ and $k_0 = -1$, (f–j) $\varepsilon = 0.002$ and $k_0 = -1$. For (a, f) $t = 10$ time units, (b, g) $t = 100$ time units, (c, h) $t = 250$ time units, (d, i) $t = 400$ time units, (e, j) $t = 500$ time units.

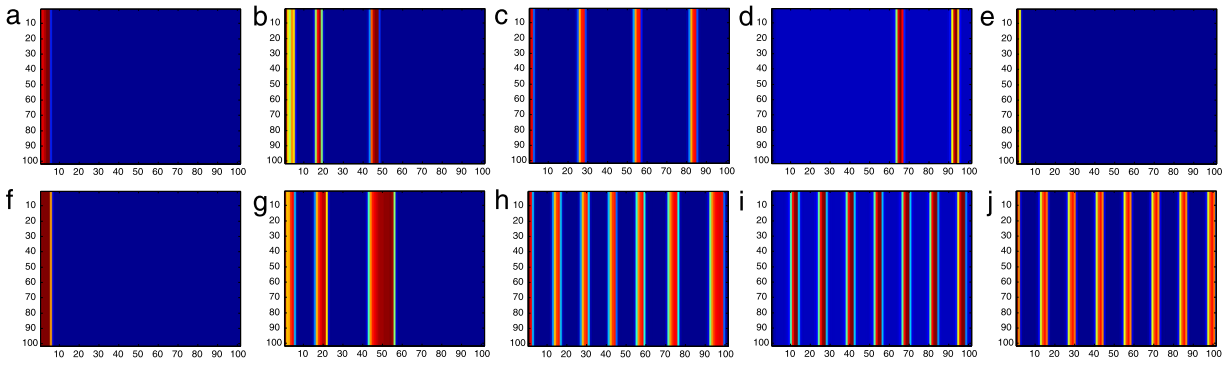

Fig. 2. Intermittent and continuous plane waves, traveling across the excitable tissue; for (a–e) $\varepsilon = 0.02$ and $k_0 = -0.5$, (f–j) $\varepsilon = 0.002$ and $k_0 = -0.5$. For (a, f) $t = 10$ time units, (b, g) $t = 100$ time units, (c, h) $t = 250$ time units, (d, i) $t = 400$ time units, (e, j) $t = 500$ time units.

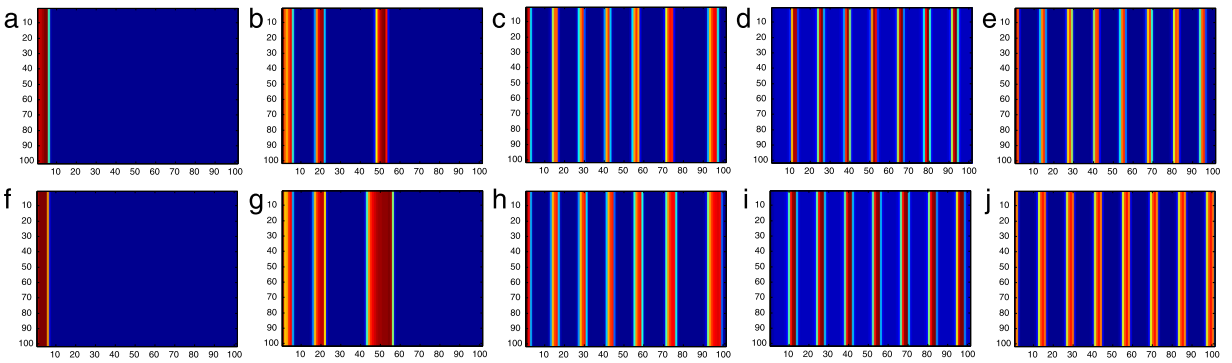

Fig. 3. Continuous plane waves, traveling across the excitable tissue; for (a–e) $\varepsilon = 0.02$ and $k_0 = 0.5$, (f–j) $\varepsilon = 0.002$ and $k_0 = 0.5$. For (a, f) $t = 10$ time units, (b, g) $t = 100$ time units, (c, h) $t = 250$ time units, (d, i) $t = 400$ time units, (e, j) $t = 500$ time units.

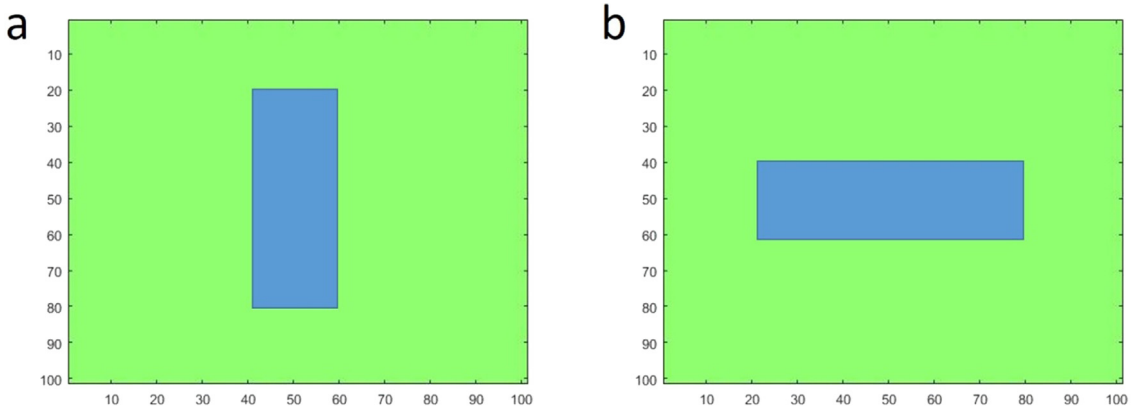

Fig. 4. Coordination of the rectangular obstacle in the excitable tissue. (a) vertical obstacle, (b) horizontal obstacle.

2. Mathematical model of the tissue

In the context of mathematical neuronal models, some models are presented including the ionic models like Hodgkin–Huxley (HH) model [24] and Noble model [25], and the simplified models like Karma model [26], Fitzhugh–Nagumo (FHN) model [27], Barkley model [28], Hindmarsh—Rose model [29], etc. Mathematical modeling of the cardiac tissue is a valuable tool that has grown significantly since 1962 when Denis Noble modified the equations formulated by Hodgkin–Huxley in 1952. The Noble model is the first mathematical model of cardiac action potentials and pacemaker rhythms [25]. From one perspective, given the nonlinearity and the complexity of the heart, the simplified models are more noticed to investigate the qualitative characteristics of the heart's dynamics. The advantage of this attitude is that these models permit analytical analysis [30]. In addition, although being simplified, these models have been successful to reproduce some generic properties of such complex demonstrations [31]. The FHN model, which is derived as the simplification of the HH equations, can reproduce generic characteristics of the neurons and cardiac fibers. This model includes excitation threshold and refractory period. Some modified versions of the FHN model are also presented. For example, Aliev and Panfilov [30] proposed a two-variable model describing the fast and the slow processes. The model is described by the following equations:

$$\begin{aligned} \frac{du}{dt} &= D_u \nabla^2 u - ku\,(u-a)\,(u-1) - uv \\ \frac{dv}{dt} &= \left(\varepsilon + \frac{v\mu_1}{u+\mu_2}\right)(-v - ku(u-a-1)) \end{aligned} \tag{1}$$

where u (fast variable) and v (slow variable) are the transmembrane potential and the ion current, respectively. The right-hand side of the first equation of Eq. (1) is similar to the original FHN model [30]. Parameter $a = 0.15$ is the threshold for excitation and $k = 8$ is dependent on the media. The nonlinear term $-ku\,(u-a)\,(u-1) - uv$ is the total transmembrane current per unit area [32]. The Laplacian operator in two-dimensional space is $\nabla^2 = \partial_{xx} + \partial_{yy}$. Parameter $D_u = 1$ is the

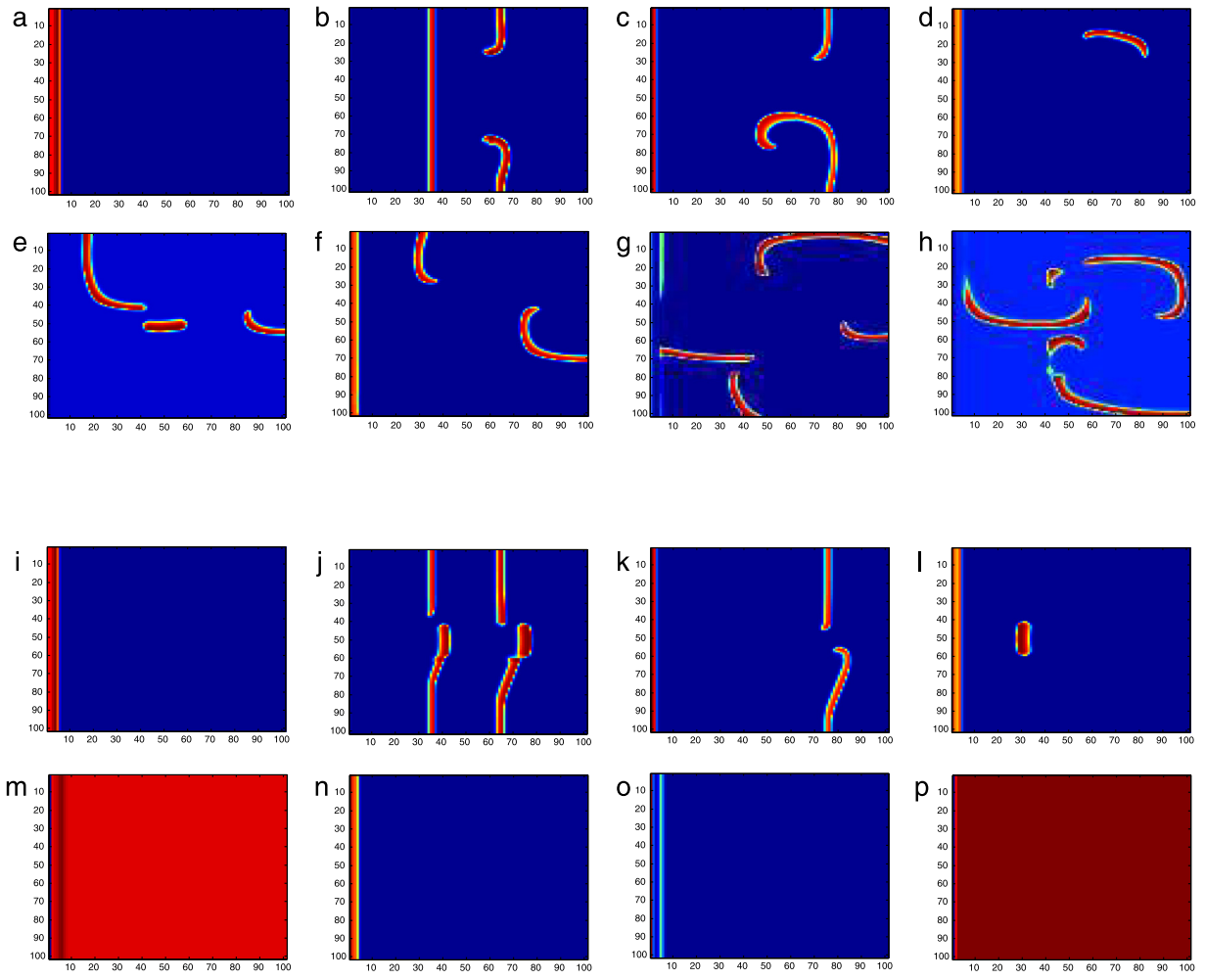

Fig. 5. Spatiotemporal patterns from the wavefront-obstacle interaction, for $\varepsilon = 0.02$, $k_0 = -1$, in the presence of (a–h) the vertical obstacle, and (i–p) the horizontal obstacle. For (a, i) $t = 10$ time units, (b, j) $t = 150$ time units, (c, k) $t = 250$ time units, (d, l) $t = 350$ time units, (e, m) $t = 450$ time units, (f, n) $t = 600$ time units, (g, o) $t = 700$ time units, (h, p) $t = 800$ time units.

diffusion coefficient. The parameters $\mu_1 = 0.2$ and $\mu_2 = 0.3$ are fixed, and the parameter ε is often used to describe the excitability of the media.

Although this model is well capable of reproducing different generic behaviors of the neuron, some effective factors are missed. For instance, the continuous exchange of the ions across the membrane brings a time-varying electrical field, and thus a time-varying magnetic field. This varying magnetic force mutually affects the electrical activity of the ions. There is also some evidence that the electromagnetic field changes the gap junction communication [33]. Based on these facts, in this study, we use the mathematical model in which a magnetic flux variable is considered [32]. This additive variable describes the magnetic flux induced by the distribution of the ion concentration. The enhanced three-variable model is as follows:

$$\begin{aligned} \frac{du}{dt} &= D_u \nabla^2 u - ku\,(u-a)\,(u-1) - uv + k_0 \rho(\phi) u \\ \frac{dv}{dt} &= \left(\varepsilon + \frac{v\mu_1}{u+\mu_2}\right)(-v - ku(u-a-1)) \\ \frac{d\phi}{dt} &= k_1 u - k_2 \phi \\ \rho\,(\phi) &= \frac{dq(\phi)}{d\phi} = \alpha + 3\beta\phi^2 \end{aligned} \tag{2}$$

where the additive variable ϕ describes the magnetic flux across the membrane. The term $k_0\rho(\phi)u$ is the induction current induced by electromagnetic induction [32] and the parameter k_0 modulates the magnetic induction on the membrane

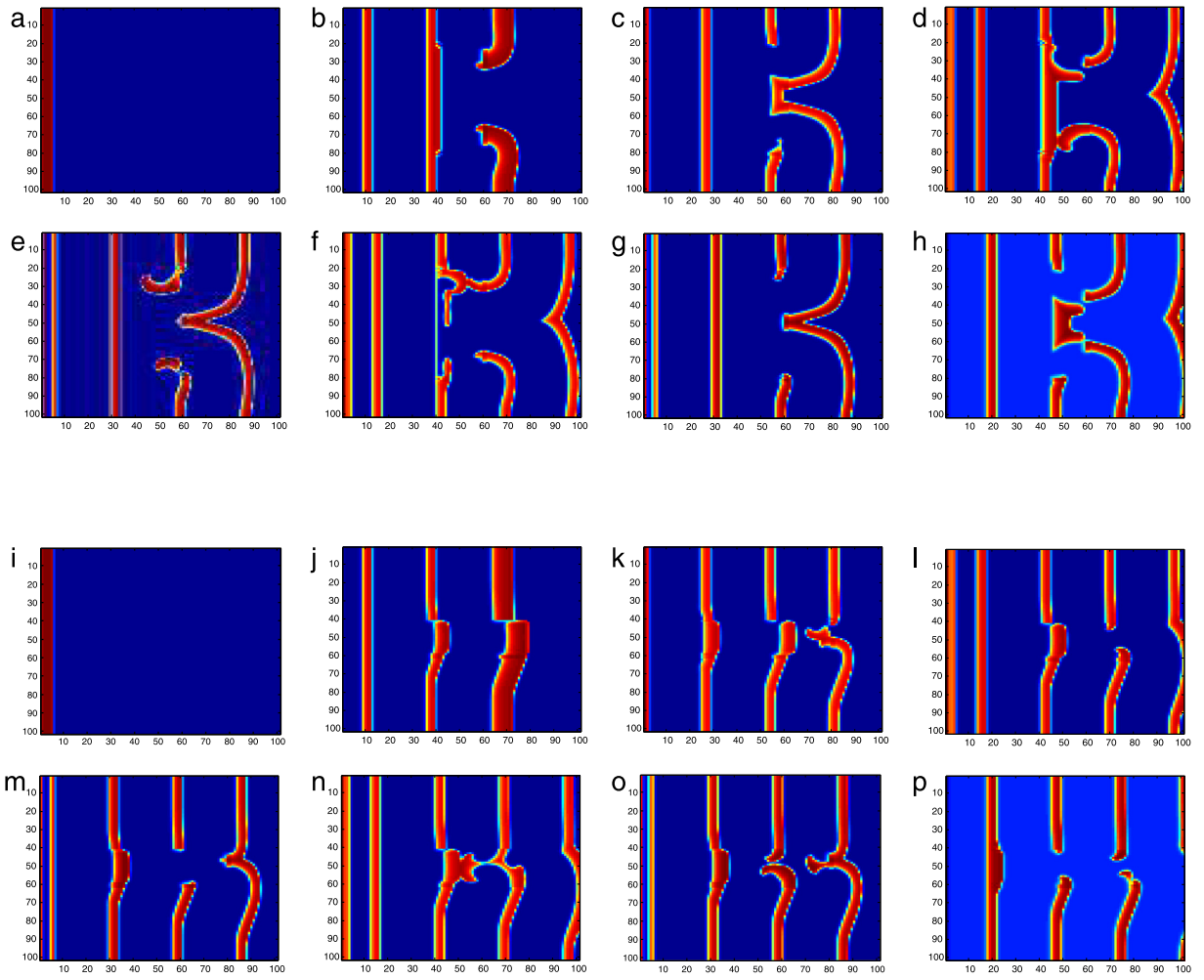

Fig. 6. Spatiotemporal patterns from the wavefront-obstacle interaction, for $\varepsilon = 0.002$, $k_0 = -1$, in the presence of (a–h) the vertical obstacle, and (i–p) the horizontal obstacle. For (a, i) $t = 10$ time units, (b, j) $t = 150$ time units, (c, k) $t = 250$ time units, (d, l) $t = 350$ time units, (e, m) $t = 450$ time units, (f, n) $t = 600$ time units, (g, o) $t = 700$ time units, (h, p) $t = 800$ time units.

potential. The parameters $k_1 = 0.2$ and $k_2 = 1$ adjust the electromagnetic effect induced by the ion exchange in the cell and the saturation of the magnetic flux, respectively.

In this study we design a lattice consisting of 101×101 neurons, as a model of the cardiac tissue. The local dynamics of each neuron is governed by Eq. (2). Furthermore, we consider the 4-neighbor connection for all the neurons of the lattice (see Eq. (3)). We consider the excitable media using the following equations:

$$\begin{aligned}
\frac{du_{ij}}{dt} &= -ku_{ij}\left(u_{ij}-a\right)\left(u_{ij}-1\right) - u_{ij}v_{ij} + k_0\rho\left(\phi_{ij}\right)u_{ij} + D_u\left(u_{i+1j} + u_{i-1j} + u_{ij+1} + u_{ij-1} - 4u_{ij}\right) + f\delta_{i\eta}\delta_{j\zeta} \\
\frac{dv_{ij}}{dt} &= \left(\varepsilon + \frac{v_{ij}\mu_1}{u_{ij}+\mu_2}\right)\left(-v_{ij} - ku_{ij}(u_{ij}-a-1)\right) \\
\frac{d\phi_{ij}}{dt} &= k_1u_{ij} - k_2\phi_{ij} \\
\rho\left(\phi_{ij}\right) &= \alpha + 3\beta\phi_{ij}^2
\end{aligned} \tag{3}$$

where ij shows the location of each neuron in the lattice ($(1 \le i \le 101$ and $1 \le j \le 101$; $i, j \in \mathbb{z})$. $\delta_{i\eta} = 1$ for $i = \eta$ and $\delta_{i\eta} = 0$ for $i \ne \eta$, $\delta_{j\zeta} = 1$ for $j = \zeta$ and $\delta_{j\zeta} = 0$ for $j \ne \zeta$. $f = A\cos(\omega t)$ is a periodic force applying to the tissue's left boundary by $\eta = 1$: 101 and $\zeta = 1$. The parameters $A = 0.6$ and $\omega = 0.2$ are fixed.

3. Numerical simulation and discussion

In this section, the interaction of wavefront-obstacle is investigated by the numerical method. We consider a square network of 101×101 neurons as an excitable tissue. We apply a periodic force on the boundary of the tissue to generate successive wavefronts, and then we put an obstacle toward the path of wave propagation to see their interaction. On the other hand, the excitability of the tissue plays a decisive role for the traveling wavefronts to continue or stop. It means that the excitability of the tissue can hinder the traveling plane waves in the tissue, even in the presence of periodic force on the boundary. Given this, three cases can happen: (1) the excitability of the tissue is high enough to support the wave propagation, so that the successive plane waves travel across the tissue during the whole time span (Fig. 1f–j, Fig. 2f–j, Fig. 3); (2) the excitability of the tissue is not very high, so that some traveling plane waves take place but not continuously (Fig. 1a–e, Fig. 2a–e); (3) the tissue does not support wave propagation due to its low excitability. It is important to consider the two states of continuous and intermittent propagation of the plane waves. Because as soon as a spiral seed emerges in the tissue, it can get to the power if there are no continuous plane waves. It means that the continuous propagation of the plane waves can impede the growth of the spiral wave in the tissue. The Figs. 1–3 show the results of different levels of excitability, made by different adjustments of the two parameters ε and k_0. In the FHN model, as mentioned earlier, the first variable is the fast variable, which excites the neuron. Given Eq. (3), the excitatory variable can increase by intensifying the induction current, which is adjustable by the parameter k_0. On the other hand, the second variable of the FHN model is the inhibitory variable. In this study, we use the parameter ε to vary the inhibitory strength. In fact, the tissue's excitability decreases by increasing the parameter ε. We aim to represent different possible patterns arise from the interaction between the plane waves and the obstacle. First, we modulate the tissue's excitability by setting the parameters ε and k_0, and then we show how much it can support the plane waves propagation for each case (Figs. 1–3). Note that no obstacle is considered in these figures. Second, we put the obstacle in the central area of the tissue and compare the results. The parameters setting for these figures are given in Table 1.

Now let us consider a slice of cardiac tissue with an obstacle. We place the obstacle by making different excitability properties in a specific area with Neumann boundary conditions at its edges. The mechanism of the initiation of reentry and thus the spatial perturbation in the wave pattern caused by the heterogeneity is well documented in the literature. However, the orientation of the obstacle is also important. Therefore, we examine the rectangular obstacle in both horizontal and vertical orientation, and generate the plane waves from the tissue's left boundary for each case. In this way, we will see which orientation disturbs the propagation pattern more significantly. Fig. 4 shows the coordination of both the vertical and the horizontal obstacle that we consider in the present work. The wavefront-obstacle interaction is shown in some snapshots over the time to track the development of the resulting spatiotemporal patterns. We found that the initiation of reentry and formation of the spiral waves are highly probable near the boundary of the obstacle. Moreover, the plane waves can greatly be broken depending on the obstacle's orientation. In addition, the continuity of the traveling wavefronts, which is dependent on the tissues excitability, in turn, influences the final spatial pattern. In this regard, we examine both horizontal and vertical orientation of the obstacle for each level of the tissue's excitability.

In Fig. 5, the parameters are set as $\varepsilon = 0.02$ and $k_0 = -1$. Fig. 5 shows how the plane waves generated from the left boundary undergo the changes that lead to a completely different pattern from what can be seen in Fig. 1a–e. In Fig. 1a–e, the traveling plane waves exist only in a limited time span and after that, there is no traveling plane wave (Fig. 1d,e). However, Fig. 5a–h shows that the propagation does not stop affected by the vertical obstacle. The obstacle makes a proper condition for the initiation of reentry, and then the spiral waves emerge in the tissue. Furthermore, Fig. 5i–p shows the resulting pattern for a horizontal obstacle in the tissue during the time. In this case, spiral seeds have the less opportunity to emerge, so that the tissue's electrical activity becomes synchronized after a limited time (Fig. 5m–p).

As mentioned earlier, the continuity of the successive plane waves is also determinative for the resulting spatial pattern and should be investigated. To this end, we decrease the value of parameter ε, from $\varepsilon = 0.02$ to $\varepsilon = 0.002$, so that the tissue becomes more excitable, and thus it supports continuous traveling plane waves. The related successive plane waves in absence of the obstacle are shown in Fig. 1f–j. Having the tissue with this level of excitability, we place the obstacle in the tissue to see the wavefront-obstacle interaction. The upper snapshots of Fig. 6 (Fig. 6a–h) represent the result for vertical obstacle over the time, while the lower snapshots (Fig. 6i–p) display the results for the horizontal obstacle. It is found that the plane waves can go around the horizontal obstacle in a way that leads to less spatial perturbation in the final pattern (compare Fig. 6h and p).

Moreover, the interaction of the plane waves shown in Fig. 2a–e with the obstacle is displayed in Fig. 7, where $\varepsilon = 0.02$ and $k_0 = -0.5$. Fig. 7a–h shows that, with this excitability level, the effect of vertical obstacle gives rise to the emergence of spiral wave inside the obstacle. The resulting spiral wave is trammeled by the obstacle's borders and cannot rule it out. Actually, it continues to rotate as long as possible, while there is no other force to suppress it. Thus, the tissue is prevented from the synchronized electrical activity. In contrast, the tissue gets synchronized by placing a horizontal obstacle in the tissue (see Fig. 7n–p). Actually, the horizontal obstacle leads to formation of some spiral seeds at the obstacle's edges. However, the seeds do not maintain in the tissue because of the rectangle's orientation relative to the wave propagation direction.

After that, we investigate this case for the successive wavefronts shown in Fig. 2f–j, in which the plane waves are continuously propagated. To this end, we place the obstacle in the tissue while reducing the parameter ε from $\varepsilon = 0.02$ to $\varepsilon = 0.002$ (see Fig. 8). The snapshots of Fig. 8a–h, in which the vertical obstacle is considered, confirm that the formation of

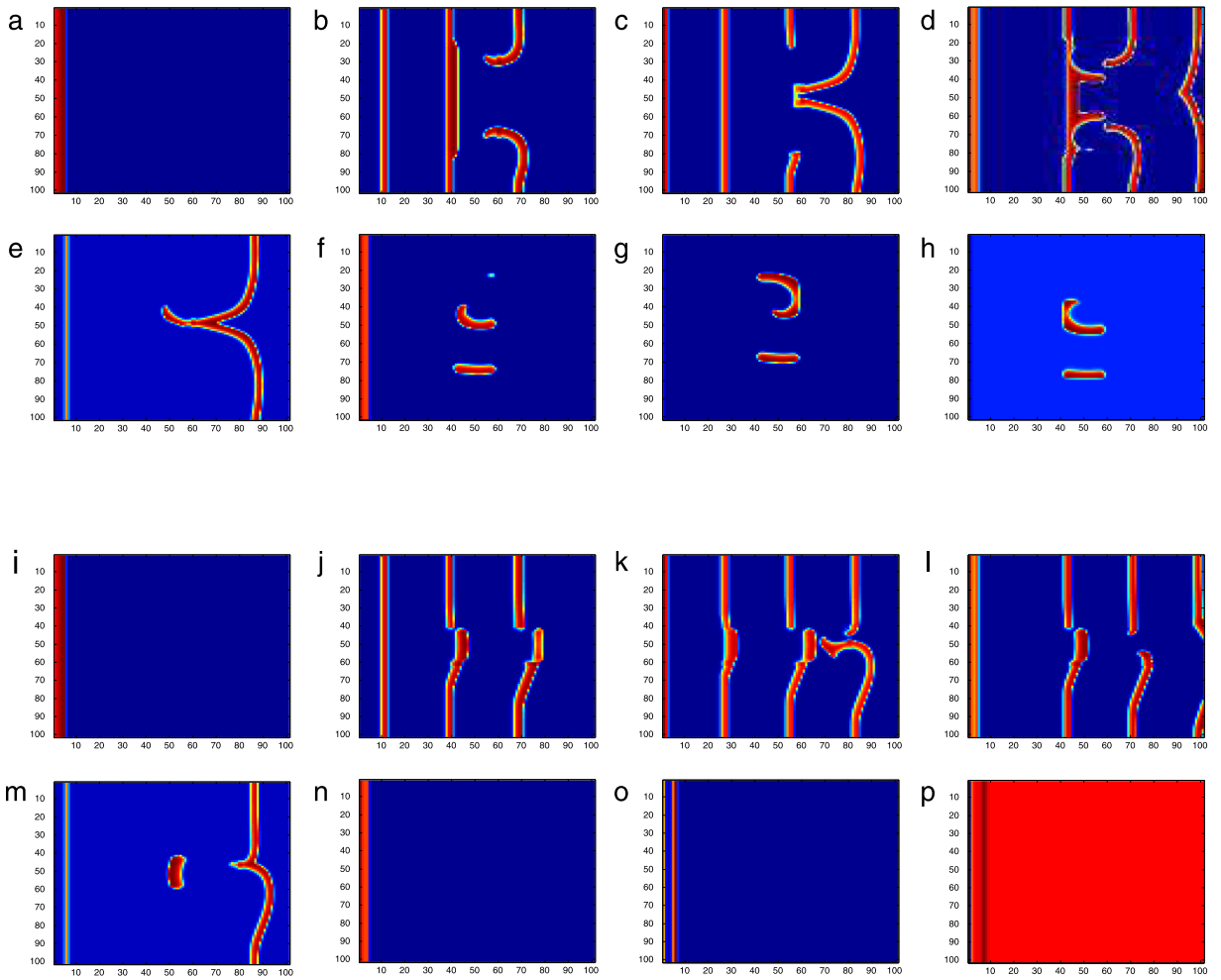

Fig. 7. Spatiotemporal patterns from the wavefront-obstacle interaction, for $\varepsilon = 0.02$, $k_0 = -0.5$, in the presence of (a–h) the vertical obstacle, and (i–p) the horizontal obstacle. For (a, i) $t = 10$ time units, (b, j) $t = 150$ time units, (c, k) $t = 250$ time units, (d, l) $t = 350$ time units, (e, m) $t = 450$ time units, (f, n) $t = 600$ time units, (g, o) $t = 700$ time units, (h, p) $t = 800$ time units.

perfect spiral wave suffers from consecutive wavefronts. Therefore, some imperfect spirals co-exist with the broken traveling plane waves. In fact, each segment of the broken plane waves starts bending from its ends that gives rise to the spiral seed. Furthermore, this co-existence also takes place when we replace the vertical obstacle with a horizontal one (Fig. 8i–p). However, the difference between the results of Fig. 8a–h and Fig. 8i–p is in the amount of spatial perturbation in the tissue. Actually, the point is that, a wider section of the obstacle is placed toward the wave propagation direction by putting the vertical obstacle. Therefore, the spiral arm can become longer since the ends of each segment of the broken wavefront's are more distant from each other. Consequently, the vertical obstacle brings more deformation in the spatial pattern than the horizontal one.

For the last step, we seek to discover the resulting spatiotemporal pattern in a highly excitable tissue caused by both the intensified induction current and the reduced parameter ε. As is illustrated in Fig. 3, the tissue well conducts the wavefronts by setting $k_0 = 0.5$, so that all the generated pulses from the tissue's left boundary can reach out the other side. Regarding this state of the tissue, we place the obstacle in the tissue to see the resulting pattern (Fig. 9). By putting the vertical obstacle (Fig. 9a–h), even though the ends of the broken plane waves are distant from each other, the resulting spiral waves cannot grow perfectly due to the high spatial frequency of the successive plane waves. That is to say, formation of each spiral wave does not complete since its spiral arm immediately meets the subsequent wavefront and gets suppressed. In fact, the frequent plane waves give rise to multiple spirals by reaching the obstacle. These multiple spiral seeds rotate with different frequencies and get broken. In addition, the resulting spatial perturbation expands over the time (Fig. 9e–h). However, the same as before, this spatial perturbation caused by the horizontal obstacle is less than the vertical one (Fig. 9i–p).

As explained earlier, the other tool to increase the tissue's excitability is to reduce the inhibitory effect. In this regard, we set $\varepsilon = 0.002$ for all the neurons in the lattice. By this adjustment, the frequent wavefronts become stronger and the

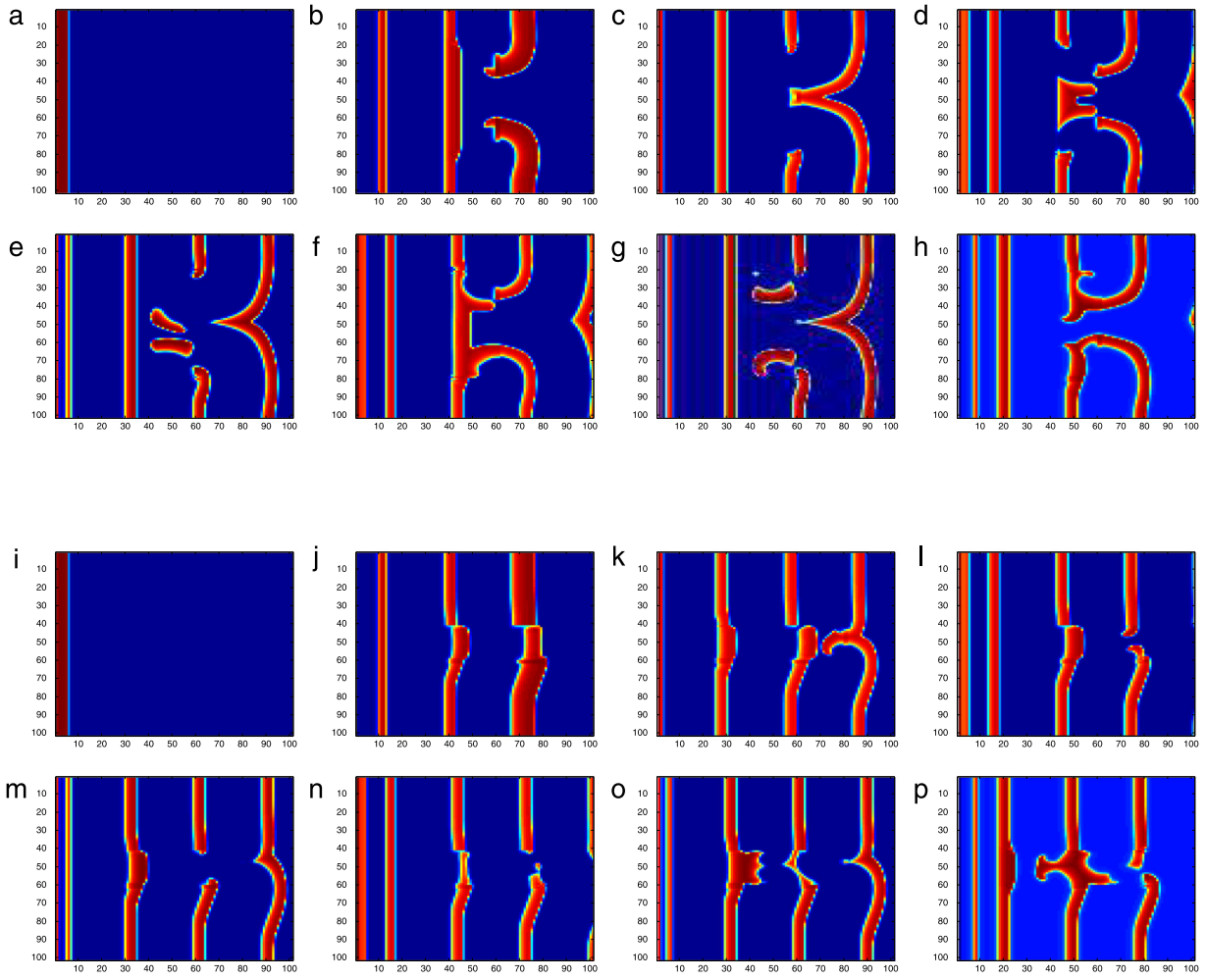

Fig. 8. Spatiotemporal patterns from the wavefront-obstacle interaction, for $\varepsilon = 0.002$, $k_0 = -0.5$, in the presence of (a–h) the vertical obstacle, and (i–p) the horizontal obstacle. For (a, i) $t = 10$ time units, (b, j) $t = 150$ time units, (c, k) $t = 250$ time units, (d, l) $t = 350$ time units, (e, m) $t = 450$ time units, (f, n) $t = 600$ time units, (g, o) $t = 700$ time units, (h, p) $t = 800$ time units.

two ends of the broken plane waves perfectly follow the obstacle's borders (Fig. 10). Moreover, the curved stripe pattern, which is primarily organized from the initial plane waves, stays for a longer time when the vertical obstacle is considered (Fig. 10a–h). In addition, his particular pattern co-exists with some slight imperfect spiral waves. Furthermore, we also surveyed the changes of wave pattern under the effect of horizontal obstacle (Fig. 10i–p). It is found that, the spatial pattern is more robust in the presence of the horizontal obstacle when the tissue is highly excitable. Here the internal ends of the two segments of the broken plane waves perfectly follow the horizontal borders of the obstacle. This interaction between the obstacle and the plane waves postpones the reentry and the spiral waves.

4. Conclusion

In this work, a study of the initiation of reentry and the formation of spiral waves in a model of the cardiac tissue with an obstacle was represented. We used a modified FHN model in which the magnetic flux was considered. Because in the real neuron, the continuous exchange of the ions across the membrane causes a time-varying magnetic field, and this magnetic field mutually affects the membrane's electrical activity. Therefore, the new FHN model would be more reliable, while it holds an additive variable of magnetic flux and also more bifurcation parameters.

On the other hand, the induction current affecting the neuron's membrane potential and the inhibitory property of the neuron's dynamics are the two factors that we used in our work to adjust the tissue's excitability. In fact, the tissue's excitability plays a decisive role in propagation of the generated wavefronts. In this context, three cases could happen: (1) the excitability of the tissue is high enough to support the wave propagation, so that the successive plane waves travel across the tissue, continuously; (2) the excitability of the tissue is not very high, so that some traveling plane waves take place but not continuously; (3) the tissue does not support wave propagation due to its low excitability. Given this, to investigate

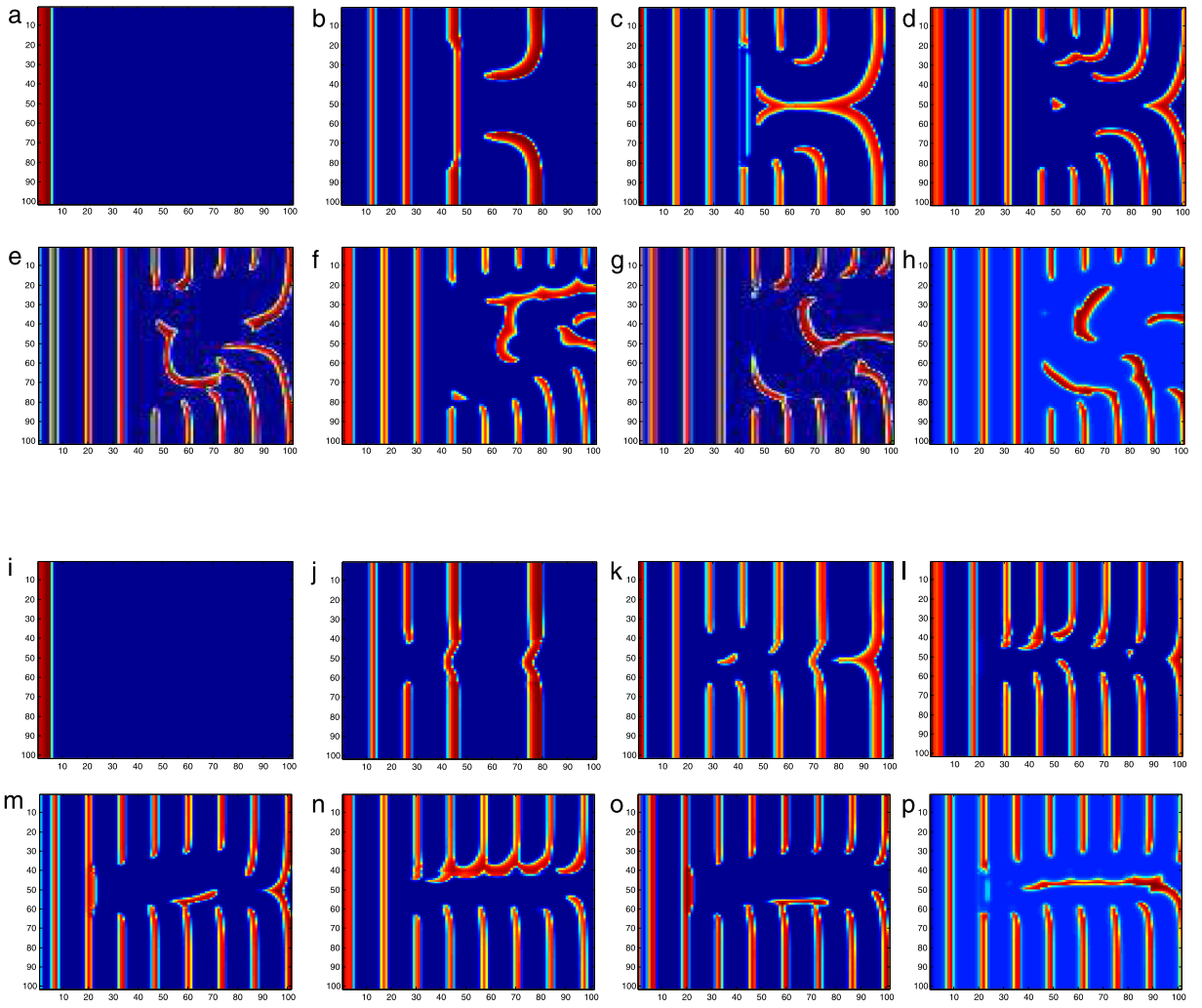

Fig. 9. Spatiotemporal patterns from the wavefront-obstacle interaction, for $\varepsilon = 0.02$, $k_0 = 0.5$, in the presence of (a–h) the vertical obstacle, and (i–p) the horizontal obstacle. For (a, i) $t = 10$ time units, (b, j) $t = 150$ time units, (c, k) $t = 250$ time units, (d, l) $t = 350$ time units, (e, m) $t = 450$ time units, (f, n) $t = 600$ time units, (g, o) $t = 700$ time units, (h, p) $t = 800$ time units.

the wavefront-obstacle interaction, we placed a rectangular obstacle in the tissue in the presence of both continuous and intermittent traveling waves. Our investigation reveals that the interaction of the wavefront-obstacle gives rise to reentry, and thus to the emergence of spiral wave. The results showed that the reentrant excitation took place near the obstacle's borders and potentially led to multi-spirals in that area. The multi-spirals co-existed with the successive plane waves that resulted in a gradually expanding perturbation area. In addition, the obstacle could also hold a perfect spiral wave under specific circumstances. This was while the tissue became synchronized in its normal state, in which there was no obstacle. We picked the two vertical and horizontal obstacles to see the effect of obstacle's orientation relative to the propagation direction on the resulting patterns. It is found that a wider section of the obstacle toward the wave propagation direction brings more deformation for the spatial pattern. Confirming this, a horizontal obstacle caused less perturbation, so that the wavefronts generated from one side of the tissue could reach out the opposite side with less deformation. Furthermore, aside from the obstacle's orientation, the strength and the continuity of the successive plane waves also determined the resulting spatial pattern. It actually could postpone the reentry, which in turn, caused less deformation in the normal spatial pattern. The high excitability of the tissue causes the plane waves transfer easier in the tissue. These plane waves could follow the obstacle's borders after getting broken, and the striped spatial pattern was more robust against spatial deformation.

Acknowledgments

Sajad Jafari was supported by the Iran National Science Foundation (Grant No. 96000815). Matjaž Perc was supported by the Slovenian Research Agency, Slovenia (Grant nos. J1-7009 and P5-0027).

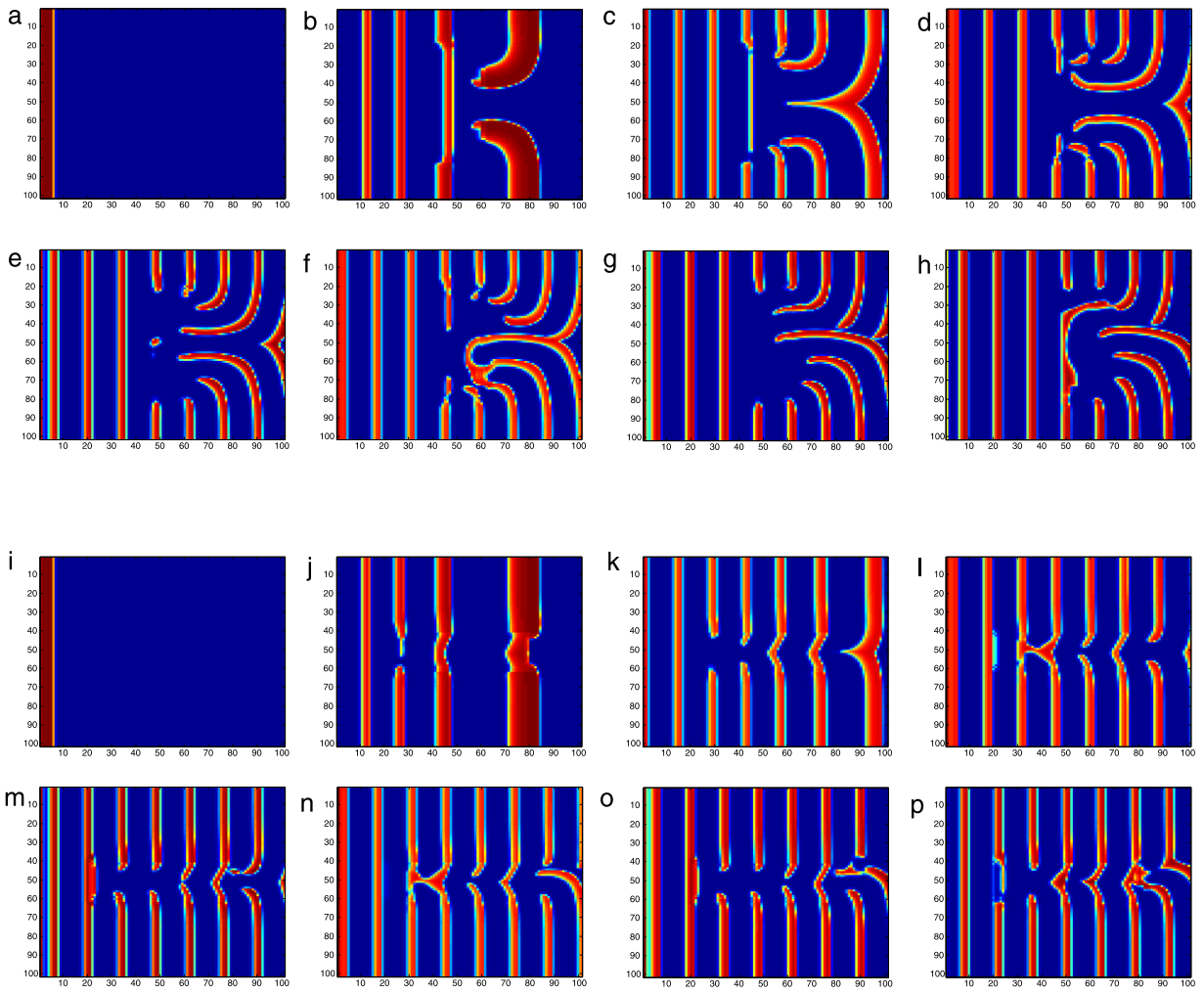

Fig. 10. Spatiotemporal patterns from the wavefront-obstacle interaction, for $\varepsilon = 0.002$, $k_0 = 0.5$, in the presence of (a–h) the vertical obstacle, and (i–p) the horizontal obstacle. For (a, i) $t = 10$ time units, (b, j) $t = 150$ time units, (c, k) $t = 250$ time units, (d, l) $t = 350$ time units, (e, m) $t = 450$ time units, (f, n) $t = 600$ time units, (g, o) $t = 700$ time units, (h, p) $t = 800$ time units.

References

[1] M.R. Guevara, et al., George Ralph Mines (1886–1914): the dawn of cardiac nonlinear dynamics, J. Physiol. 594 (9) (2016) 2361–2371.
[2] A.V. Panfilov, J.P. Keener, Effects of high frequency stimulation on cardiac tissue with an inexcitable obstacle, J. Theoret. Biol. 163 (4) (1993) 439–448.
[3] J.M. Starobin, et al., Wavelet formation in excitable cardiac tissue: the role of wavefront-obstacle interactions in initiating high-frequency fibrillatory-like arrhythmias, Biophys. J. 70 (2) (1996) 581–594.
[4] J. Ma, et al., Defects formation and wave emitting from defects in excitable media, Commun. Nonlinear Sci. Numer. Simul. 34 (2016) 55–65.
[5] F. Xie, Z. Qu, A. Garfinkel, Dynamics of reentry around a circular obstacle in cardiac tissue, Phys. Rev. E 58 (5) (1998) 6355.
[6] D.J. Christini, L. Glass, Introduction: Mapping and control of complex cardiac arrhythmias, Chaos 12 (3) (2002) 732–739.
[7] L. Campanari, et al., Varieties of reentrant dynamics, Chaos 27 (4) (2017) 041101.
[8] M. Perc, M. Gosak, M. Marhl, Periodic calcium waves in coupled cells induced by internal noise, Chem. Phys. Lett. 437 (1–3) (2007) 143–147.
[9] F. Wu, et al., Multi-channels coupling-induced pattern transition in a tri-layer neuronal network, Physica A 493 (2018) 54–68.
[10] M. Perc, Effects of small-world connectivity on noise-induced temporal and spatial order in neural media, Chaos Solitons Fractals 31 (2) (2007) 280–291.
[11] X. Sun, M. Perc, J. Kurths, Effects of partial time delays on phase synchronization in Watts–Strogatz small-world neuronal networks, Chaos 27 (5) (2017) 053113.
[12] L.D. Weise, A.V. Panfilov, Discrete Mechanical Modeling of Mechanoelectrical Feedback in Cardiac Tissue: Novel Mechanisms of Spiral Wave Initiation, in: Modeling the Heart and the Circulatory System, Springer, 2015, pp. 29–50.
[13] A.V. Panfilov, Spiral breakup as a model of ventricular fibrillation, Chaos 8 (1) (1998) 57–64.
[14] J.M. Davidenko, et al., Stationary and drifting spiral waves of excitation in isolated cardiac muscle, Nature 355 (6358) (1992) 349.
[15] T. Ikeda, et al., Attachment of meand, ering reentrant wave fronts to anatomic obstacles in the atrium: role of the obstacle size, Circ. Res. 81 (5) (1997) 753–764.
[16] Y.-H. Kim, et al., Role of papillary muscle in the generation and maintenance of reentry during ventricular tachycardia and fibrillation in isolated swine right ventricle, Circulation 100 (13) (1999) 1450–1459.

[17] A.M. Pertsov, et al., Spiral waves of excitation underlie reentrant activity in isolated cardiac muscle, Circ. Res. 72 (3) (1993) 631–650.
[18] D. Olmos-Liceaga, Spiral waves, obstacles and cardiac arrhythmias, in: Cardiac Arrhythmias-New Considerations, InTech, 2012.
[19] D. Olmos-Liceaga, H. Ocejo-Monge, On the generation of spiral and scroll waves by periodic stimulation of excitable media in the presence of obstacles of minimum size, Chaos Solitons Fractals 99 (2017) 162–170.
[20] J. Zhang, et al., The dynamics of spiral tip adjacent to inhomogeneity in cardiac tissue, Physica A 491 (2018) 340–346.
[21] Z.Y. Lim, et al., Spiral wave attachment to millimeter-sized obstacles, Circulation 114 (20) (2006) 2113–2121.
[22] C.A. Athill, et al., Transmembrane potential properties at the core of functional reentrant wave fronts in isolated canine right atria, Circulation 98 (15) (1998) 1556–1567.
[23] J. Cysyk, L. Tung, Electric field perturbations of spiral waves attached to millimeter-size obstacles, Biophys. J. 94 (4) (2008) 1533–1541.
[24] A.L. Hodgkin, A.F. Huxley, A quantitative description of membrane current and its application to conduction and excitation in nerve, J. Physiol. 117 (4) (1952) 500–544.
[25] D. Noble, A modification of the Hodgkin—Huxley equations applicable to Purkinje fibre action and pacemaker potentials, J. Physiol. 160 (2) (1962) 317–352.
[26] A. Karma, Spiral breakup in model equations of action potential propagation in cardiac tissue, Phys. Rev. Lett. 71 (7) (1993) 1103.
[27] R. FitzHugh, Impulses and physiological states in theoretical models of nerve membrane, Biophys. J. 1 (6) (1961) 445–466.
[28] D. Barkley, A model for fast computer simulation of waves in excitable media, Physica D 49 (1–2) (1991) 61–70.
[29] J. Hindmarsh, R. Rose, A model of the nerve impulse using two first-order differential equations, Nature 296 (5853) (1982) 162.
[30] R.R. Aliev, A.V. Panfilov, A simple two-variable model of cardiac excitation, Chaos Solitons Fractals 7 (3) (1996) 293–301.
[31] D.A. Kessler, H. Levine, W.N. Reynolds, Theory of the spiral core in excitable media, Physica D 70 (1–2) (1994) 115–139.
[32] F. Wu, et al., Model of electrical activity in cardiac tissue under electromagnetic induction, Sci. Rep. 6 (1) (2016) 28.
[33] E. Fear, M. Stuchly, A novel equivalent circuit model for gap-connected cells, Phys. Med. Biol. 43 (6) (1998) 1439.